Author/s:
Tayebi, M;O'Rorke, R;Wong, HC;Low, HY;Han, J;Collins, DJ;Ai, Y

Title:
Massively Multiplexed Submicron Particle Patterning in Acoustically Driven Oscillating Nanocavities

Date:
2020-04-28

Citation:
Tayebi, M., O'Rorke, R., Wong, H. C., Low, H. Y., Han, J., Collins, D. J. & Ai, Y. (2020). Massively Multiplexed Submicron Particle Patterning in Acoustically Driven Oscillating Nanocavities. Small, 16 (17), https://doi.org/10.1002/smll.202000462.

Persistent Link:
https://hdl.handle.net/11343/275553

Massively multiplexed sub-micron particle patterning in acoustically driven oscillating nanocavities

Mahnoush Tayebi[1†], Richard O'Rorke[1†], Him Cheng Wong[1], Hong Yee Low[1], Jongyoon Han[2,3], David J. Collins[4*], Ye Ai[1*]

[1]Pillar of Engineering Product Development, Singapore University of Technology and Design, Singapore 487372, Singapore

[2]Department of Biological Engineering, Massachusetts Institute of Technology, Cambridge, MA 02139, USA

[3]Department of Electrical Engineering and Computer Science, Massachusetts Institute of Technology, Cambridge, MA 02139, USA

[4]Department of Biomedical Engineering, The University of Melbourne, Melbourne, VIC 3010, Australia

[†]These authors contributed equally to this work

Corresponding authors*

Email: aiye@sutd.edu.sg, Tel: (+65) 6499 4553

Email: david.collins@unimelb.edu.au, Tel: (+61) 3 8344 0867

Abstract

This is the author manuscript accepted for publication and has undergone full peer review but has not been through the copyediting, typesetting, pagination and proofreading process, which may lead to differences between this version and the Version of Record. Please cite this article as doi: 10.1002/smll.202000462.

Nanoacoustic fields are a promising method for particle actuation at the nanoscale, though THz frequencies are typically required to create nanoscale wavelengths. In this work we demonstrate the generation of robust nanoscale force gradients using MHz driving frequencies via acoustic-structure interactions. A structured elastic layer at the interface between a microfluidic channel and a travelling surface acoustic wave (SAW) device results in sub-micron acoustic traps, each of which can trap individual sub-micron particles. The acoustically-driven deformation of nanocavities gives rise to time-averaged acoustic fields which direct suspended particles towards, and trap them within, the nanocavities. The use of SAWs permits massively multiplexed particle manipulation with deterministic patterning at the single-particle level. In this work, 300-nm-diameter particles are acoustically trapped in 500-nm-diameter cavities using travelling SAWs with wavelengths in the range of 20–80 μm with one particle per cavity. On-demand generation of nanoscale acoustic force gradients has wide application for nanoparticle manipulation, including bioparticle enrichment and enhanced catalytic reactions for industrial applications.

Keywords: Submicron particle manipulation; Acoustofluidics; Nanocavity; Surface Acoustic waves; Nanoacoustics

1. Introduction

The growing use of nanoparticles and sub-micron particles in various applications, including engineering [1], nanomaterial fabrication[2, 3], biology[4, 5] and medicine[6], requires high-throughput particle manipulation for preparation, enrichment and quality control. For example, the size distribution of synthesized nanoparticle catalysts determines their catalysis efficiency[7, 8]. In biomedical applications, exosomes, which are sub-micron extracellular vesicles[9-11] containing DNA, microRNAs and proteins, are a potential source of diagnostic biomarkers[12-15]. Suitable nanoparticle manipulation tools would enable size-based sorting/filtering, or manipulation towards downstream activities such as multiplexed

diagnostics, nanoelectronic/robotic constructions[16, 17] and nanoparticle-based drug delivery systems[18]. Conventional particle separation techniques[19] are based on differential density and size, for example ultracentrifugation[20], ultrafiltration[21] and size exclusion chromatography[22]. Although impressive progress has been made in the last decade, many nanoparticle manipulation tools suffer from high cost, low throughput and specimen damage[23-25]. Scalable nano- and sub-micron particle patterning has thus traditionally relied on self-assembly methods[26] or oligomer templating[27] however, these are largely unable to produce deterministic single-nanoparticle positioning, they are irreversible, and they require specific reagents or lengthy processing[28-30]. Moreover, drug delivery systems which incorporate efficient nanoparticle concentration are creating new avenues for cancer treatment[31, 32]. There is, therefore, a pressing need to develop a fast, precise and scalable method for nano- and sub-micron scale manipulation.

Microfluidic devices have emerged as a viable platform for particle manipulation using magnetic[33], optoelectronic[34], plasmonic[35], electrokinetic[36] and hydrodynamic[37] forces. Applying these principles at the nanoscale instead of the microscale, however, can result in far smaller force magnitudes, poor separation efficiency and channel clogging[38]. Furthermore, most of these manipulation methods are constrained by their dependence on particle polarizability, the need for low conductivity medium (which is often not biocompatible), and heating of the surrounding fluid. Optical tweezers[39, 40] provide the highest degree of spatial resolution but they are usually applied in static fluids, owing to the relatively small forces that can be generated[41], and only small numbers of nanoparticles can be manipulated at any one time (those within the field of a focused optical beam[42-44]). Acoustic fields have been widely used for micron-scale particle manipulation, employing either bulk acoustic waves (where a resonance mode of a rigid microchannel is excited) or surface acoustic waves (where an acoustic wave travels along the surface of a piezoelectric substrate and couples into an adjoining microchannel), to produce a non-zero time-averaged pressure field in the channel which affects an acoustic radiation force on suspended particles. Whilst acoustic nanoparticle manipulation has been demonstrated using MHz frequencies[45-48], single nanoparticle positioning has not been demonstrated.

In an instance of acoustic nanoparticle manipulation, Raeymaekers *et al*.[49] used bulk acoustic waves to position suspended diamond nanoparticles at the nodal positions of a standing bulk acoustic wave in a cylindrical reservoir. More recently, Tung *et al*.[50] employed a viscoelastic layer enclosing air cavities above a bulk transducer to spatially modulate the acoustic wavefront amplitude and produce near-field potential wells to pattern microparticles and cells into clusters with 50 μm resolution.

Although BAW-based devices generally enable handling larger fluid volumes and throughputs[51-53], SAW devices are advantageous for precise micromanipulation since they can achieve higher frequencies[45, 54], can readily localize the acoustic fields in specific regions[38, 55, 56], and are a well-established method for the precise spatial control of particles[57]. Periodic patterns of suspended particles are typically formed using standing surface acoustic waves (SSAWs)[58-61], though we recently demonstrated particle patterning using travelling SAWs via near-field interference patterns formed near channel boundaries and in-channel features[62-64]. The dissipation of acoustic energy in a liquid leads to acoustic streaming (a time-averaged motion of the bulk liquid), resulting in a dominance of viscous drag forces over acoustic radiation forces for particles below a critical size, which can prevent acoustic trapping[65, 66]. This critical particle size is frequency dependent, and has restricted the use of acoustic fields for manipulation of individual nanoscale objects, which would otherwise be useful in fields including sensing (plasmonic nanoparticles[67]), optics (micro-lenses[68]) and computation (circuits from sintered particles[69]). Nanoacoustic methodologies, specifically those involving acoustic field gradients at sub-micron scales, nevertheless present a promising avenue for nano and sub-micron particle manipulation, although their primary use has been imaging[70] and nanoscale detection[71] rather than actuation.

In this work, we develop a novel acoustofluidic manipulation method to simultaneously direct millions of sub-micron particles into discrete, single particle traps. In doing so, we overcome the hitherto inseparable coupling between the applied acoustic wavelength and the length scale of the resulting force gradients. Microfluidic channels are used to contain a sub-micron particle solution atop an array of patterned nanocavities, beneath which is a travelling SAW device. Upon application of a

travelling SAW, nanocavity deformations are induced via oscillatory displacements of the underlying SAW device, which couple to the surrounding fluid to generate time-averaged pressure fields which direct suspended particles towards pressure minima via acoustic radiation forces, as illustrated in Figure 1. Travelling SAWs produce non-zero, time-averaged pressure fields which can direct particles in the direction of wave propagation[63, 72] or towards local minima of a near field interference pattern. Here, however, the oscillating nanocavities give rise to local minima in the time-averaged pressure field within each nanocavity, to which suspended particles are directed by an acoustic radiation force. Utilizing SAW wavelengths between 20-80 μm, nanoscale acoustic gradients are generated in the vicinity of individual nanocavities, successfully trapping individual 300-nm-diameter particles inside 500-nm-diameter cavities with the application of a travelling SAW.

2. Material and Methods

The nanoacoustic patterning device comprises three principle components: the SAW substrate, the nanopatterned polymeric layer and the microchannel. Supplementary Figure S1 (a) and (b) shows the complete acoustofluidic chip fabrication process and a photograph of the chip, respectively. The SAW substrate is 128° rotated Y-cut, X propagating lithium niobate ($LiNbO_3$), patterned with interdigitated electrodes (IDTs) which were deposited via electron-beam evaporation of a 5-nm-thick chromium adhesion layer and a 100-nm-thick conductive gold layer. The number of electrode finger-pairs was calibrated to minimize the electrical impedance mismatch with a 50 Ω signal generation source, with 30, 27, 18, 12 and 7 finger-pairs for 80, 40, 20, 10 and 5 μm SAW wavelengths, respectively, each with an 800-μm-wide IDT aperture. The corresponding applied frequencies were 49, 98, 196, 389, 778 MHz.

The nanocavities were formed by imprinting NOA73 (Norland Optical Adhesive, Norland Products, USA) directly on the SAW device using a mold made from polydimethylsiloxane (PDMS) and crosslinking by UV exposure (900 mJ/cm^2 at 350 nm). The PDMS mold was patterned from a silicon

master as described previously[73]. Briefly, the silicon master template was attached to a casting jig enclosing a casting cavity into which PDMS (SYLGARD® 184, Aldrich) with an elastomer to crosslinker ratio of 10:1 was then poured, degassed and cured at 80°C for a minimum of 2 hours. The silicon master consisted a hexagonal array of 500-nm-diameter pillars with a 1 μm pitch.

The PDMS microchannel was fabricated by soft-lithography using a silicon/SU8 master with channel features defined by photolithography. The channel height was 3.5 μm. The PDMS microchannel was bonded to the NOA73 nanocavity layer via silanisation of the PDMS using (3-aminopropyl) triethoxylsilane (APTES) functionalization[74]. Briefly, the PDMS microchannel was exposed to an air plasma (Harrick Plasma PDC-32G; 1000 mTorr, 18 W) for 50 seconds followed by immersion in an APTES (Aldrich, Singapore) solution for 5 minutes. The PDMS microchannel was then rinsed in water and dried before being aligned with the nanocavity layer under a stereomicroscope, with the microchannels aligned parallel to the IDT finger-pairs, after which the entire device was heated at 150°C for 1 hour. The temperature was ramped at 2°C/min and a pressure of 0.35 N/cm^2 was maintained to prevent debonding due to different thermal expansion coefficients.

The particle trapping during the SAW "on" phase and release during the SAW "off" phase was monitored using a fluorescence microscope (CKX53 OLYMPUS, USA). A 0.1% w/v suspension of fluorescent polystyrene particles with diameter of 300 nm and coefficient of variation of 3% (Magsphere, USA) and surfactant (1% w/v, F-127) was injected into an array of 60-μm-wide, parallel microchannels spaced 40 μm apart. A particle diameter of 300 μm was the smallest that we could resolve with conventional fluorescence microscopy, meaning each 500-nm-diamter cavity accommodated only a single nanoparticle. The microchannels were filled at a flowrate of 1 μL/min using a syringe pump (KD Scientific, Holliston, MA). A high-frequency signal generator (Rigol DSG815, Beijing, China) and a broadband amplifier (qianmei Standard 1-930 MHz 2W RF Broadband Power Amplifier) were used to generate sinusoidal electrical signals (0.1 mW applied power). The morphology and thickness of the nanoimprinted NOA73 layer were measured using scanning electron microscopy (SEM; JEOL JSM-7600F). In order to visualize trapped particles within

the nanocavities, the PDMS channels were carefully peeled from the NOA73 layer immediately after exposure to the SAW, with the exposed NOA73 layer removed from the SAW device using a small metal chisel, transferred to conductive carbon tape and dried at room temperature overnight prior to SEM imaging.

To understand the origin of the nanoacoustic patterning phenomena, we employed a 2D finite element model, illustrated in Supplementary Figure S2, in which the time-averaged pressure field, $\langle p \rangle$, in a liquid channel located on top of the nanocavity array was calculated. The nanocavity layer was modelled as a linear elastic material under conditions of plane strain with the parameters given in Table 1. The travelling SAW was applied via a velocity boundary condition with velocity $v = \omega\delta$, where δ is the displacement field of the travelling SAW[75], given in the *x* (propagation) and *y* (surface normal) directions by:

$$\delta_x = \zeta\delta_0 \left[e^{-C_d\left(\frac{W}{2}-x\right)} e^{i\left[-k\left(\frac{W}{2}-x\right)+\omega t\right]} \right] \quad (1)$$

where ζ is ratio of displacement amplitudes in the *x* and *y* directions,

and

$$\delta_y = -\delta_0 \left[e^{-C_d\left(\frac{W}{2}-x\right)} e^{i\left[-k\left[\left(\frac{W}{2}-x\right)+\omega t-\frac{\pi}{2}\right]\right]} \right]. \quad (2)$$

The wavenumber $k = 2\pi/\lambda$, W is the width of the liquid domain (centered at $x = 0$) and the SAW decay coefficient C_d is given by[75]

$$C_d = \frac{\rho_l c_l}{\rho_s c_s \lambda}, \quad (3)$$

where the subscripts l and s denote the liquid and substrate, respectively. We assume that the nanocavity layer will not significantly alter the attenuation of the travelling SAW, which is valid for layers that are acoustically thin (i.e. $h_{NP} \ll \lambda$). The $e^{i\omega t}$ terms were omitted in the frequency domain

study, where harmonic perturbations are assumed. The elastic deformation of the nanocavity layer was coupled to linear pressure waves in the liquid domain via the Helmholtz equation to calculate the time averaged pressure field, $\langle p \rangle = 0.5\sqrt{p * p}$, where the asterisk denotes complex conjugation. This model was implemented in COMSOL Multiphysics v5.0 using the Solid Mechanics and Thermoacoustic Physics interfaces. A mesh convergence study was conducted, where the convergence, C, of parameter, g, was evaluated according to Devendran *et al.*[75], with

$$C(g) = \sqrt{\frac{\int (g - g_{ref})^2 \, dxdy}{\int (g_{ref})^2 \, dxdy}}. \quad (4)$$

The model converged at a mesh density of 12 elements per λ_{SAW} (see Supplementary Figure S3).

The acoustic radiation force, F^{rad}, on a spherical particle with diameter $\ll \lambda_{\mathrm{SAW}}$ is given by[76]

$$F^{\mathrm{rad}} = -\nabla U^{\mathrm{rad}}, \quad (5a)$$

where the acoustic potential, U^{rad}, is

$$U^{\mathrm{rad}} = \frac{4\pi}{3} D^3 \left[f_1 \frac{1}{2} k_l \langle p^2 \rangle - f_2 \frac{3}{4} \rho_l \langle V^2 \rangle \right]. \quad (5b)$$

The monopole and dipole coefficients, $f_1$and f_2, are given by

$$f_1 = 1 - \frac{k_p}{k_l} \quad (5c)$$

$$f_2 = \frac{2\left(\frac{\rho_p}{\rho_l} - 1\right)}{2\frac{\rho_p}{\rho_l} + 1}, \quad (5d)$$

where k_p, ρ_p and k_l, ρ_l are compressibility and density of particles and liquid, respectively. Values of f_1 and f_2 for our system were calculated to be 0.44 and 0.03, respectively. Given the relative

magnitude of the dipole coefficients, $\langle p^2 \rangle$, was taken as a proxy measure of the acoustic radiation force. To quantify the ability of the device to convey sub-micron particles into the nanocavities, we evaluated the maximum trapping force, $F_{\max}$, according to Equation 5 in the y direction between the top of the nanocavity, $y = 0$, and $y = h_{ac}$, the first inflection point of the pressure gradient, $\delta\langle p^2 \rangle / \delta y$.; beyond h_{ac} the acoustic radiation force is not able to translate particles into the nanocavities.

3. Results and Discussion

Representative fluorescence micrographs in Figure 2 show 300-nm-diameter particles initially dispersed in a suspension, individually trapped within nanocavities upon the application of a 20-µm-wavelength (196 MHz) travelling SAW and subsequently released with the cessation of SAW excitation. Particle migration from the bulk fluid into the nanocavities is also shown in Supplementary Video S1. The simulated pressure field, $\langle p^2 \rangle$, taken as a proxy for the acoustic radiation force, is plotted in Figure 3(a), and shows acoustic pressure nodes within each nanocavity and the direction of the pressure gradient is indicated by arrows. The unique nanoscale pattern of the time-averaged pressure field arises from indirect coupling of the travelling SAW into the liquid channel via the deformable polymeric film; these deformations are examined in detail later. To evaluate the dependence of particle capture on the acoustic wavelength, we performed experiments and simulations for 10, 20, 40, and 80 µm wavelengths. Simulated pressure fields are given in Figure 3(b), which show distinct deformation modes at different acoustic wavelengths; for wavelengths ≥ 20 µm, particles will be directed towards pressure nodes within the nanocavities, whilst with a 10 µm wavelength the pressure gradient will repel particles from the nanocavities. In addition, we note that the pressure field is not uniform across the channel and is lower near the channel walls, meaning trapping will proceed faster in the channel centre than near the walls. These results are consistent with our experimental observations of sub-micron particle capture at different acoustic wavelengths (see Figure 4), where 5 and 10-µm-wavelengths do not generate appreciable particle trapping, in contrast

to the SAW wavelengths ≥ 20 μm. In Figure 4, the few empty nanocavities for SAW wavelengths ≥ 20 μm likely arose from the statistical nature of the trapping in which particles randomly filled the nanocavities according to their position in the flow.

Whilst most nanocavities contain a pressure node, actually trapping a particle inside the cavity requires a pressure gradient that slopes towards the cavity, to direct a suspended particle from the bulk liquid into the cavity. To examine this trapping mechanism, we evaluated the acoustic radiation force, F, as a function of distance in the y direction from the top of the nanocavity (for the central nanocavity in the simulation domain). Example data are shown for $\lambda = 20$ μm in Figure 5a. From this data we calculated two parameters to quantify the trapping ability of the nanocavities: the effective acoustic range, h_{ac}, defined as the distance between the top of the nanocavity and the first inflection point of the acoustic radiation force, F, and the maximum acoustic radiation force, $F_{\max}$, in the negative y direction (i.e. towards the nanocavity). These parameters were evaluated for the same nanocavity device perturbed by a travelling SAW with wavelengths, λ, from 18 to 50 μm. The effective acoustic range, h_{ac}, and the maximum acoustic radiation force, $F_{\max}$, are plotted as a function of λ in Figure 5b and c. Although the effective acoustic range decreases nonlinearly with increasing λ, indicating that shorter wavelengths (or higher applied frequencies) are preferable for particle capture, $F_{\max}$ shows well-defined maxima at discreate frequencies. The dependencies of effective trapping range and trapping force on acoustic wavelength fully support our experimental observations that particle trapping does not occur for 5 and 10-μm-wavelengths, is most prominent at a 20 μm wavelength and occurs more slowly at higher wavelengths, as evidenced in Supplementary Videos S1 and S2. By examining the change in width of the central nanocavity, $\tilde{\xi}$, as a function of λ (see Figure 5d) we see that the $F_{\max}$ maxima correspond to resonance modes of the nanocavities where the nanocavity oscillates in an expansion/contraction mode (see inset in Figure 5d), where:

$$\tilde{\xi} = \frac{w_{\max} - w_0}{w_0}, \qquad (7)$$

and w_o is the unperturbed nanocavity width.

SEM images of nanocavities are given in Figure 6, showing both empty nanocavities before particle trapping and nanocavities populated with acoustically trapped particles. Incomplete nanocavity filling and particle fouling of the nanocavity layer is likely caused by particle release during sample handling, since the number of fouling particles corresponds to the number of empty nanocavities.

We have presented a technique that decouples the wavelength of a travelling SAW from the length scale of the resulting pressure gradients (which give rise to acoustic radiation forces) by coupling the travelling SAW through an intermediate layer patterned with nanocavities. This offers distinct advantages over particle manipulation using surface acoustic waves (either travelling or standing wave) and bulk acoustic waves. Firstly, the location of trapped particles is determined entirely by the location of cavities in the removable nanocavity layer, and not by fixed parameters such as the acoustic wavelength, channel dimensions or location, size and shape of the channel features[77]. Also, the number of particles held in each location is determined by the ratio of cavity size to particle size, and not by the ratio of acoustic wavelength to particle size[78]. In this work, we chose a cavity to particle diameter ratio of 0.6, but ratios from 0.5–1 may also be suitable to capture a single particle per cavity.

Whilst deterministic single-particle trapping has recently been demonstrated for 7–10-μm-diameter particles[60, 79-82] and cells[54, 83, 84] with acoustic wavelengths on the order of 20–30μm, this work represents an order-of-magnitude reduction in particle size and allows a level of control over nanocavity locations (thus trapped particles) that is not possible with SAWs alone. Furthermore, our work improves on recent reports of nanoparticle capture such as nanoparticle aggregates formed using BAWs[49] and via interference patterns using air cavity waveguides[50], by patterning particles at the single particle level.

We anticipate this work will have application in areas where capture and analysis of individual nano-specimens is of importance. For example, the optical examination of extracellular vesicles (exosomes, microvescicles and apototic bodies)[85], may be facilitated by confining them in discrete points within

the 2D plane of a nanocavity array. Furthermore, our technique may be used to filter particles with diameters less than the cavity diameter, allowing deterministic size-based separation of, for example, extracellular vesicles which have different physiological functions at different sizes[86]. Other potential applications include particle concentration (without ultracentrifugation) and the formation of functional nano-patterned materials (i.e., catalytic particles and nucleation sites) when this patterning is combined with, for example, post-capture UV-curing in a resin pre-polymer solution. Whereas patterning at this scale for functional nanomaterials typically requires wetting and chemistry-based self-assembly techniques[87, 88], a deterministic method for single-nanoparticle patterning such as the one introduced here affords a far more flexible approach for creating defined patterns.

4. Conclusion

Acoustofluidics has emerged as a promising tool for micromanipulation activities at the single-particle level. Given the scaling of acoustic radiation forces and acoustic streaming velocities with increasing frequency, there are inherent difficulties in using nanoscale wavelengths for nanomanipulation. To circumvent this limitation, we have created nanoscale force gradients at microscale acoustic wavelengths by employing a nanostructured intermediate layer. The induced deformation of the nanocavities generates highly localized pressure gradients which drive sub-micron particle migration into nanocavities, as shown by finite element simulations and demonstrated in our experimental setups. These pressure gradients can overcome Brownian motion, lateral flow and acoustic streaming to trap particles within the nanocavities. Numerical modelling reveals an optimum acoustic wavelength for rapid particle capture, corresponding to maximum deformations of the nanocavity itself, which was confirmed by experimental particle trapping at different acoustic wavelengths. Furthermore, both the effective acoustic range and the magnitude of the acoustic radiation force are wavelength dependent, with the latter exhibiting resonance modes corresponding to expansion/contraction deformation modes of the nanocavities. These resonance modes are likely to be

sub-harmonics of the nanocavity geometry and, as such, related to the mechanical and structural properties of the nanocavity layer. For the 500-nm-diameter nanocavities used here, the peak acoustic radiation force was obtained for a wavelength of 20 μm (corresponding to an applied frequency of 196 MHz), for which the effective acoustic range was 1.3μm, or 38%, of the channel height. Whilst acoustic streaming may convey particles in the upper regions of the channel into the effective trapping region, the flow rate and acoustic aperture will limit the time particles are exposed to the acoustic field, thus we anticipate a channel height comparable with the effective trapping range will be crucial for rapid particle trapping.

This work constitutes a scalable method for massively multiplexed and on-demand organising of individual sub-micron particles into discrete, single particle traps, with the potential for widespread application in sorting, patterning and size-selective capture of sub-micron and nanoscale objects. For instance, as a biomedical application, this approach may be applied in a size-based sorting of different sub-types of extracellular vesicles including exosomes (<300 nm), microvesicles (<1 μm) and apoptotic bodies (>1 μm).

Acknowledgements

This work was supported by Singapore Ministry of Education Academic Research Fund Tier 2 (T2MOE1603) awarded to Y.A.

Figures

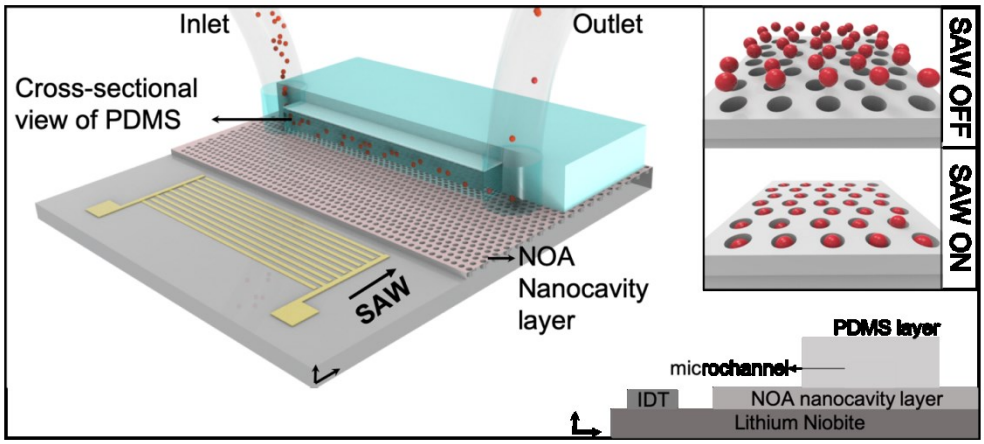

Figure 1. Acoustic nanocavity trapping concept. The acoustic trapping system is comprised of a nanocavity layer between a SAW device and a PDMS microchannel. With the application of a travelling wave SAW (SAW ON), nanoscale acoustic forces are generated that cause nanoparticle migration into nanocavities at the single-particle level.

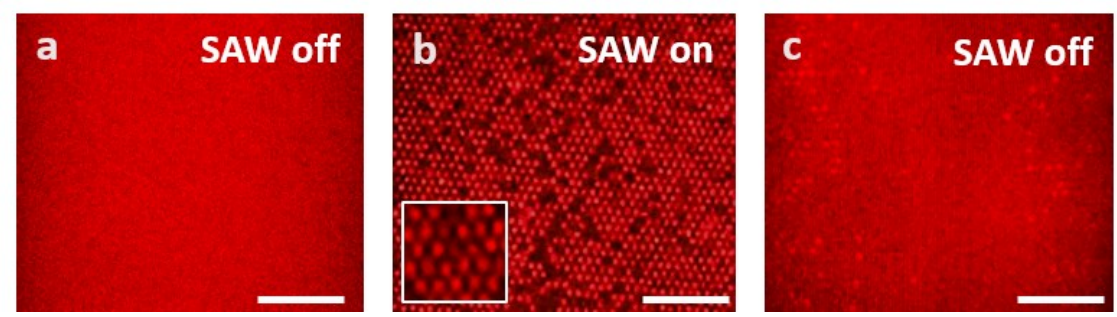

Figure 2. Acoustic trapping of 300-nm-diameter particles in acoustic nanocavities. (a) In the initial (SAW off) state, the particles are uniformly distributed throughout the microchannel. (b) With the application of SAW, nanoparticle capture is observed over a period of time (here showing 9 minutes after exposure). (c) Acoustically-trapped nanoparticles are released within a minute of discontinuing SAW excitation. The SAW wavelength and frequency are 20 µm and 196 MHz, respectively. Scale bars are 10 µm and width of the inset in panel (b) is ~7 µm.

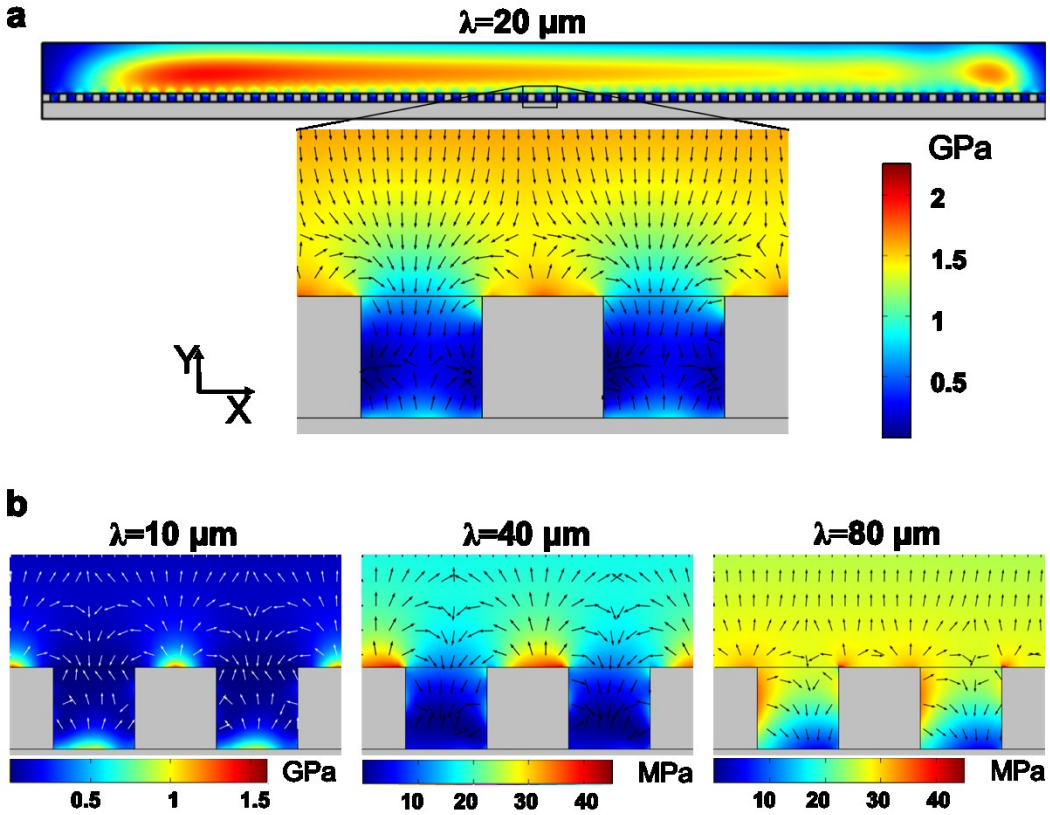

Figure 3. Plots of the square of the simulated time-averaged acoustic field, $\langle p^2 \rangle$, in a 60-μm-wide, 3.5-μm-high microchannel situated above a 1.5-μm-thick layer of NOA imprinted with 500-nm-diameter cavities (gray). (a) $\langle p^2 \rangle$ across the microchannel width, with the inset showing a close-up of the pressure field around the central nanocavity for a 20-μm-wavelength SAW. (b) $\langle p^2 \rangle$ around central nanocavities for 10, 40, and 80 μm SAW wavelengths. Arrows indicate the direction and magnitude (on a logarithmic scale) of the spatial gradient of $\langle p^2 \rangle$, which is proportional to the acoustic radiation force.

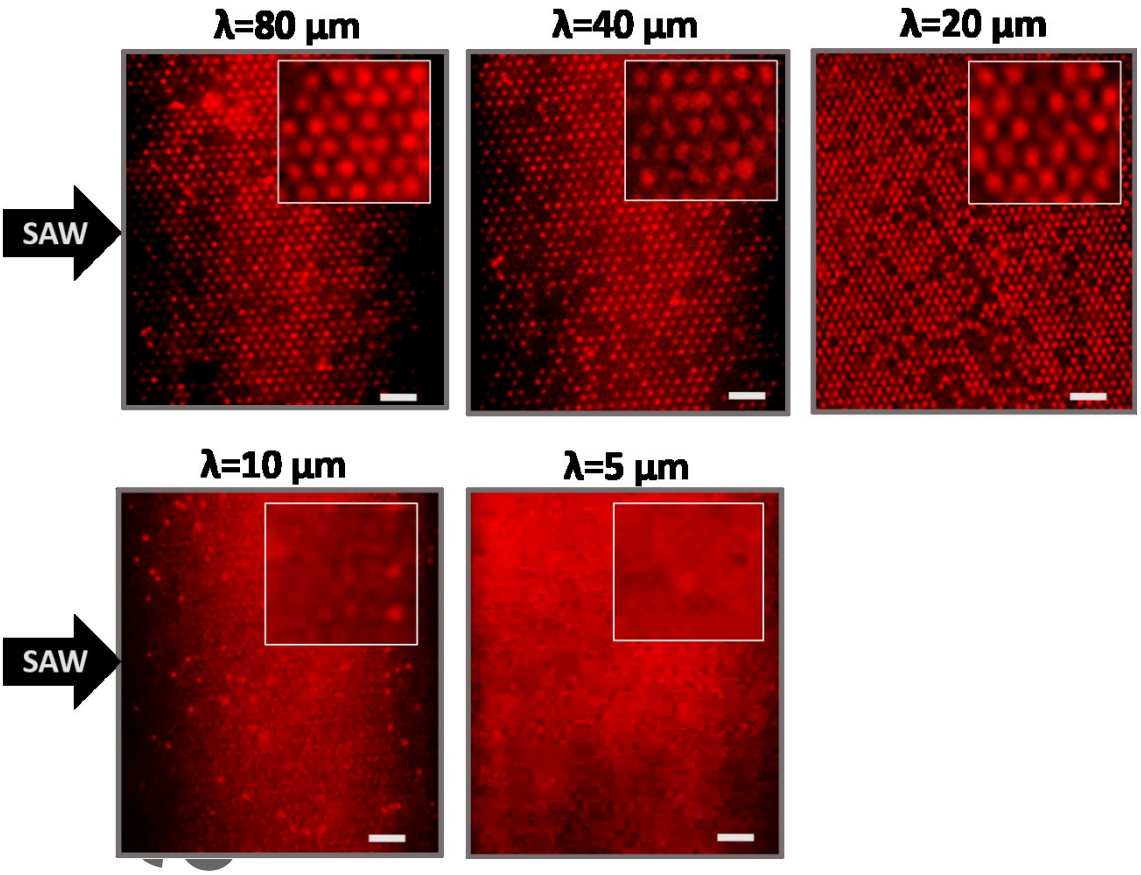

Figure 4. Fluorescence micrographs of 300-nm-diameter particles subject to a travelling SAW with wavelengths 5–80 µm with 500-nm-diameter cavities. Scale bars are 5 µm and the width of the insets is ~11 µm.

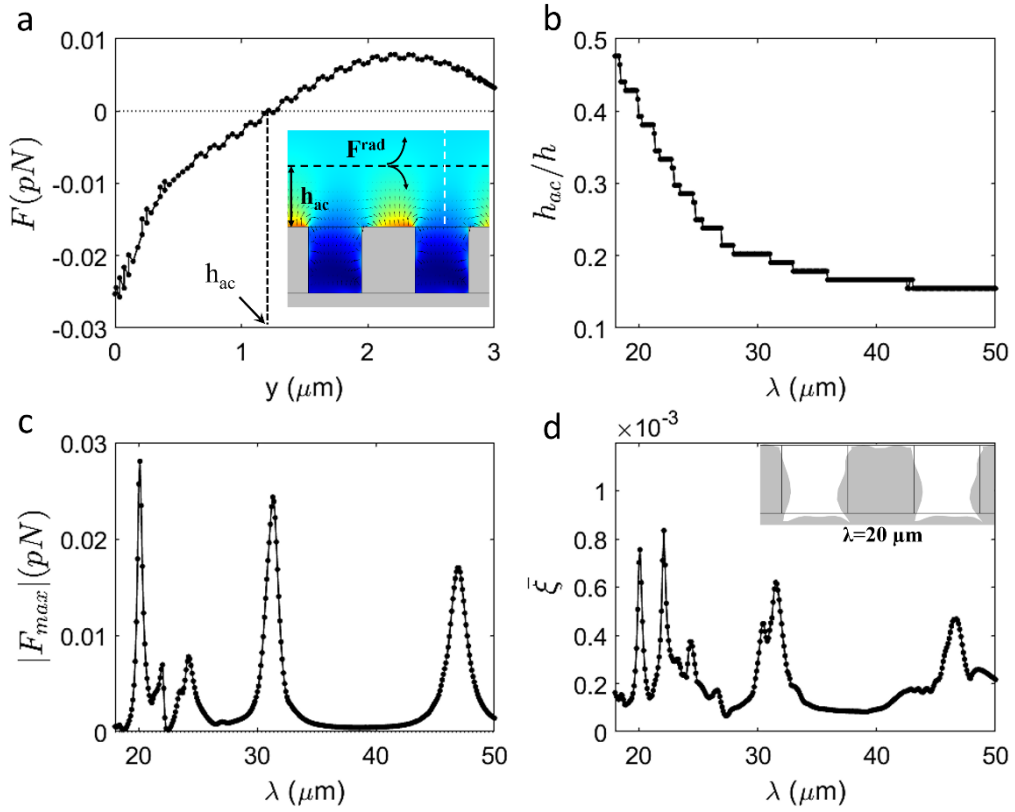

Figure 5. (a) Evaluation of the acoustic radiation force in the *y*-direction for 20 µm wavelength where h_{ac} is the distance between the top of the nanocavity and the inflection point in the pressure field gradient (white dotted line shows the *y*-range where data is evaluated). (b) Plot of the effective acoustic trapping range in y from the top of the nanocavity as a function of SAW wavelength, defined as the height above the nanocavity of the inflection point in the gradient of the pressure field, $\frac{\delta\langle p^2\rangle}{\delta y}$. (c) Plot of maximum trapping force, F_{max}, across the effective trapping range, h_{ac}; peak values correspond with maximum changes in nanocavity diameter in (d) which is quantitative comparison of the relative change in nanocavity width ($\bar{\xi}$ is derived from equation 7) in response to a travelling SAW with wavelengths in the range 18–50 µm. Insets show simulated nanocavity deformation (scaled by 10^4) for 20 µm SAW wavelengths.

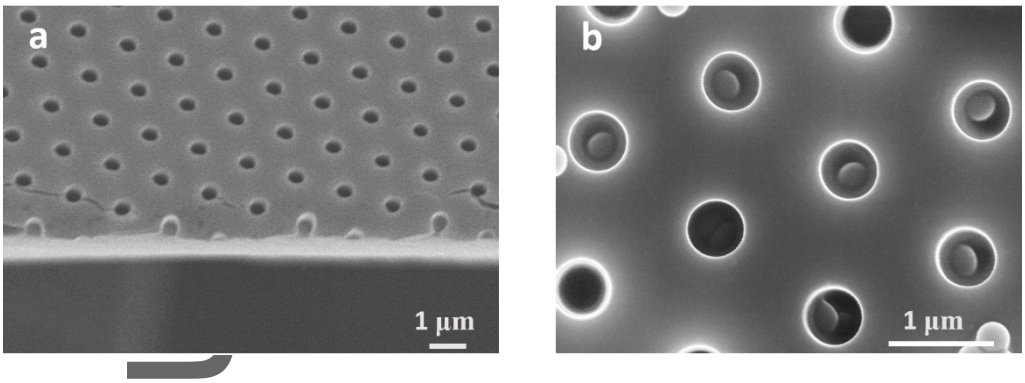

Figure 6. SEM images of nanocavities. (a) The nanocavity layer is comprised of photopolymerized NOA73 with 500 nm cavities spaced 1 µm apart. (b) Post-capture showing 300-nm-diameter particles individually trapped in single nanocavities.

Table 1. *Parameters used to simulate particle trapping in nanocavities.*

Channel width	W	60 μm
Channel height	h	3.5 μm
Acoustic wavelength	λ	20 μm
Nanocavity width	w_{pore}	500 nm
Nanocavity depth	h_{pore}	500 nm
Particle diameter	D	300 nm
Particle density	ρ_p	1050 kg/m^3

Partlcie compressibility	k_p	249 TPa^{-1}
Modus of elasticity of NOA [89]	E	~11 MPa
Density of NOA [90]	ρ	1290 Kg/m^3
Sound speed in NOA	c_p	2000 ms^{-1}
Sound speed in water	c_l	1495 ms-^{1}
Density of water	ρ_l	997 kg/m^3
Compressibility of water	k_l	448 TPa^{-1}
SAW decay length	C_d	2063 m^{-1}
SAW displacement amplitude	δ_0	0.05 nm
SAW displacement amplitude ratio [75]	ζ	0.86

References

1. Hosseinpour, M.; Fatemi, S.; Ahmadi, S. J., Catalytic cracking of petroleum vacuum residue in supercritical water media: Impact of α-Fe2O3 in the form of free nanoparticles and silica-supported granules. *Fuel* **2015,** *159*, 538-549.
2. Ma, Z.; Guo, J.; Liu, Y. J.; Ai, Y., The patterning mechanism of carbon nanotubes using surface acoustic waves: the acoustic radiation effect or the dielectrophoretic effect. *Nanoscale* **2015,** *7* (33), 14047-14054.
3. Strobl, C. J.; Schäflein, C.; Beierlein, U.; Ebbecke, J.; Wixforth, A., Carbon nanotube alignment by surface acoustic waves. *Applied Physics Letters* **2004,** *85* (8), 1427-1429.
4. Ericsson, M.; Hanstorp, D.; Hagberg, P.; Enger, J.; Nyström, T., Sorting out bacterial viability with optical tweezers. *Journal of bacteriology* **2000,** *182* (19), 5551-5555.
5. Gosse, C.; Croquette, V., Magnetic Tweezers: Micromanipulation and Force Measurement at the Molecular Level. *Biophysical Journal* **2002,** *82* (6), 3314-3329.
6. Chang, K.; Pi, Y.; Lu, W.; Wang, F.; Pan, F.; Li, F.; Jia, S.; Shi, J.; Deng, S.; Chen, M., Label-free and high-sensitive detection of human breast cancer cells by aptamer-based leaky surface acoustic wave biosensor array. *Biosensors and Bioelectronics* **2014,** *60*, 318-324.
7. Stratakis, M.; Garcia, H., Catalysis by Supported Gold Nanoparticles: Beyond Aerobic Oxidative Processes. *Chemical Reviews* **2012,** *112* (8), 4469-4506.
8. Yuan, L.; Guo, Z.; Konstantinov, K.; Liu, H.-K.; Dou, S., Nano-structured spherical porous SnO2 anodes for lithium-ion batteries. *Journal of Power Sources* **2006,** *159* (1), 345-348.
9. Raposo, G.; Stoorvogel, W., Extracellular vesicles: exosomes, microvesicles, and friends. *J Cell Biol* **2013,** *200* (4), 373-383.
10. Keller, S.; Sanderson, M. P.; Stoeck, A.; Altevogt, P., Exosomes: from biogenesis and secretion to biological function. *Immunology letters* **2006,** *107* (2), 102-108.
11. Mathieu, M.; Martin-Jaular, L.; Lavieu, G.; Théry, C., Specificities of secretion and uptake of exosomes and other extracellular vesicles for cell-to-cell communication. *Nature cell biology* **2019,** *21* (1), 9.
12. Gámez-Valero, A.; Beyer, K.; Borràs, F. E., Extracellular vesicles, new actors in the search for biomarkers for dementias. *Neurobiology of aging* **2018**.
13. Tang, M. K.; Wong, A. S., Exosomes: Emerging biomarkers and targets for ovarian cancer. *Cancer letters* **2015,** *367* (1), 26-33.
14. Ko, J.; Carpenter, E.; Issadore, D., Detection and isolation of circulating exosomes and microvesicles for cancer monitoring and diagnostics using micro-/nano-based devices. *Analyst* **2016,** *141* (2), 450-460.
15. Bellingham, S. A.; Guo, B.; Coleman, B.; Hill, A. F., Exosomes: vehicles for the transfer of toxic proteins associated with neurodegenerative diseases? *Frontiers in physiology* **2012,** *3*, 124.
16. Glotzer, S. C.; Solomon, M. J., Anisotropy of building blocks and their assembly into complex structures. *Nature Materials* **2007,** *6*, 557.
17. Auyeung, E.; Li, T. I. N. G.; Senesi, A. J.; Schmucker, A. L.; Pals, B. C.; de la Cruz, M. O.; Mirkin, C. A., DNA-mediated nanoparticle crystallization into Wulff polyhedra. *Nature* **2013,** *505*, 73.
18. Esteban-Fernández de Ávila, B.; Angell, C.; Soto, F.; Lopez-Ramirez, M. A.; Báez, D. F.; Xie, S.; Wang, J.; Chen, Y., Acoustically Propelled Nanomotors for Intracellular siRNA Delivery. *ACS Nano* **2016,** *10* (5), 4997-5005.
19. Tauro, B. J.; Greening, D. W.; Mathias, R. A.; Ji, H.; Mathivanan, S.; Scott, A. M.; Simpson, R. J., Comparison of ultracentrifugation, density gradient separation, and immunoaffinity

capture methods for isolating human colon cancer cell line LIM1863-derived exosomes. *Methods* **2012,** *56* (2), 293-304.
20. Raposo, G.; Nijman, H. W.; Stoorvogel, W.; Liejendekker, R.; Harding, C. V.; Melief, C. J.; Geuze, H. J., B lymphocytes secrete antigen-presenting vesicles. *The Journal of Experimental Medicine* **1996,** *183* (3), 1161-1172.
21. Lamparski, H. G.; Metha-Damani, A.; Yao, J.-Y.; Patel, S.; Hsu, D.-H.; Ruegg, C.; Le Pecq, J.-B., Production and characterization of clinical grade exosomes derived from dendritic cells. *Journal of Immunological Methods* **2002,** *270* (2), 211-226.
22. Novak, J. P.; Nickerson, C.; Franzen, S.; Feldheim, D. L., Purification of Molecularly Bridged Metal Nanoparticle Arrays by Centrifugation and Size Exclusion Chromatography. *Analytical Chemistry* **2001,** *73* (23), 5758-5761.
23. Li, P.; Kaslan, M.; Lee, S. H.; Yao, J.; Gao, Z., Progress in exosome isolation techniques. *Theranostics* **2017,** *7* (3), 789.
24. Trichet, A.; Dolan, P.; James, D.; Hughes, G.; Vallance, C.; Smith, J., Nanoparticle trapping and characterization using open microcavities. *Nano letters* **2016,** *16* (10), 6172-6177.
25. Ozcelik, A.; Rufo, J.; Guo, F.; Gu, Y.; Li, P.; Lata, J.; Huang, T. J., Acoustic tweezers for the life sciences. *Nature methods* **2018**, 1.
26. Hassenkam, T.; Nørgaard, K.; Iversen, L.; Kiely, C. J.; Brust, M.; Bjørnholm, T., Fabrication of 2D Gold Nanowires by Self-Assembly of Gold Nanoparticles on Water Surfaces in the Presence of Surfactants. *Advanced Materials* **2002,** *14* (16), 1126-1130.
27. Zhang, J.; Liu, Y.; Ke, Y.; Yan, H., Periodic Square-Like Gold Nanoparticle Arrays Templated by Self-Assembled 2D DNA Nanogrids on a Surface. *Nano Letters* **2006,** *6* (2), 248-251.
28. Sharma, J.; Chhabra, R.; Andersen, C. S.; Gothelf, K. V.; Yan, H.; Liu, Y., Toward Reliable Gold Nanoparticle Patterning On Self-Assembled DNA Nanoscaffold. *Journal of the American Chemical Society* **2008,** *130* (25), 7820-7821.
29. Horechyy, A.; Nandan, B.; Zafeiropoulos, N. E.; Formanek, P.; Oertel, U.; Bigall, N. C.; Eychmüller, A.; Stamm, M., A Step-Wise Approach for Dual Nanoparticle Patterning via Block Copolymer Self-Assembly. *Advanced Functional Materials* **2013,** *23* (4), 483-490.
30. Cheng, W.; Park, N.; Walter, M. T.; Hartman, M. R.; Luo, D., Nanopatterning self-assembled nanoparticle superlattices by moulding microdroplets. *Nature Nanotechnology* **2008,** *3*, 682.
31. Yavuz, M. S.; Cheng, Y.; Chen, J.; Cobley, C. M.; Zhang, Q.; Rycenga, M.; Xie, J.; Kim, C.; Song, K. H.; Schwartz, A. G.; Wang, L. V.; Xia, Y., Gold nanocages covered by smart polymers for controlled release with near-infrared light. *Nature Materials* **2009,** *8*, 935.
32. You, J.; Zhang, G.; Li, C., Exceptionally high payload of doxorubicin in hollow gold nanospheres for near-infrared light-triggered drug release. *ACS nano* **2010,** *4* (2), 1033-1041.
33. Lim, J. K.; Chieh, D. C. J.; Jalak, S. A.; Toh, P. Y.; Yasin, N. H. M.; Ng, B. W.; Ahmad, A. L., Rapid magnetophoretic separation of microalgae. *Small* **2012,** *8* (11), 1683-1692.
34. Jamshidi, A.; Pauzauskie, P. J.; Schuck, P. J.; Ohta, A. T.; Chiou, P.-Y.; Chou, J.; Yang, P.; Wu, M. C., Dynamic manipulation and separation of individual semiconducting and metallic nanowires. *Nature Photonics* **2008,** *2* (2), 86.
35. Wang, K.; Schonbrun, E.; Steinvurzel, P.; Crozier, K. B., Trapping and rotating nanoparticles using a plasmonic nano-tweezer with an integrated heat sink. *Nature Communications* **2011,** *2*, 469.
36. Cohen, A. E.; Moerner, W., Method for trapping and manipulating nanoscale objects in solution. *Applied physics letters* **2005,** *86* (9), 093109.
37. Fouet, M.; Mader, M.-A.; Iraïn, S.; Yanha, Z.; Naillon, A.; Cargou, S.; Gué, A.-M.; Joseph, P., Filter-less submicron hydrodynamic size sorting. *Lab on a Chip* **2016,** *16* (4), 720-733.
38. Collins, D. J.; Ma, Z.; Han, J.; Ai, Y., Continuous micro-vortex-based nanoparticle manipulation via focused surface acoustic waves. *Lab on a Chip* **2017,** *17* (1), 91-103.
39. Trichet, A. A. P.; Dolan, P. R.; James, D.; Hughes, G. M.; Vallance, C.; Smith, J. M., Nanoparticle Trapping and Characterization Using Open Microcavities. *Nano Letters* **2016,** *16* (10), 6172-6177.

40. Ramser, K.; Hanstorp, D., Optical manipulation for single- cell studies. *Journal of biophotonics* **2010,** *3* (4), 187-206.
41. Maragò, O. M.; Jones, P. H.; Gucciardi, P. G.; Volpe, G.; Ferrari, A. C., Optical trapping and manipulation of nanostructures. *Nature nanotechnology* **2013,** *8* (11), 807.
42. Melzer, J. E.; McLeod, E., Fundamental Limits of Optical Tweezer Nanoparticle Manipulation Speeds. *ACS Nano* **2018,** *12* (3), 2440-2447.
43. Yang, A. H. J.; Moore, S. D.; Schmidt, B. S.; Klug, M.; Lipson, M.; Erickson, D., Optical manipulation of nanoparticles and biomolecules in sub-wavelength slot waveguides. *Nature* **2009,** *457*, 71.
44. Dienerowitz, M.; Mazilu, M.; Dholakia, K., Optical manipulation of nanoparticles: a review. *Journal of Nanophotonics* **2008,** *2* (1), 1-32, 32.
45. Shilton, R. J.; Travagliati, M.; Beltram, F.; Cecchini, M., Nanoliter-Droplet Acoustic Streaming via Ultra High Frequency Surface Acoustic Waves. *Advanced Materials* **2014,** *26* (29), 4941-4946.
46. Antfolk, M.; Muller, P. B.; Augustsson, P.; Bruus, H.; Laurell, T., Focusing of sub-micrometer particles and bacteria enabled by two-dimensional acoustophoresis. *Lab on a Chip* **2014,** *14* (15), 2791-2799.
47. Li, H.; Friend, J. R.; Yeo, L. Y., Microfluidic Colloidal Island Formation and Erasure Induced by Surface Acoustic Wave Radiation. *Physical Review Letters* **2008,** *101* (8), 084502.
48. Collins, D. J.; Alan, T.; Neild, A., Particle separation using virtual deterministic lateral displacement (vDLD). *Lab on a Chip* **2014,** *14* (9), 1595-1603.
49. Raeymaekers, B.; Pantea, C.; Sinha, D. N., Manipulation of diamond nanoparticles using bulk acoustic waves. *Journal of Applied Physics* **2011,** *109* (1), 014317.
50. Tung, K.-W.; Chung, P.-S.; Wu, C.; Man, T.; Tiwari, S.; Wu, B.; Chou, Y.-F.; Yang, F.-l.; Chiou, P.-Y., Deep, sub-wavelength acoustic patterning of complex and non-periodic shapes on soft membranes supported by air cavities. *Lab on a Chip* **2019,** *19* (21), 3714-3725.
51. Dubay, R.; Lissandrello, C.; Swierk, P.; Moore, N.; Doty, D.; Fiering, J., Scalable high-throughput acoustophoresis in arrayed plastic microchannels. *Biomicrofluidics* **2019,** *13* (3), 034105.
52. Dow, P.; Kotz, K.; Gruszka, S.; Holder, J.; Fiering, J., Acoustic separation in plastic microfluidics for rapid detection of bacteria in blood using engineered bacteriophage. *Lab on a Chip* **2018,** *18* (6), 923-932.
53. Urbansky, A.; Olm, F.; Scheding, S.; Laurell, T.; Lenshof, A., Label-free separation of leukocyte subpopulations using high throughput multiplex acoustophoresis. *Lab on a Chip* **2019,** *19* (8), 1406-1416.
54. Collins, D. J.; Morahan, B.; Garcia-Bustos, J.; Doerig, C.; Plebanski, M.; Neild, A., Two-dimensional single-cell patterning with one cell per well driven by surface acoustic waves. *Nature Communications* **2015,** *6*, 8686.
55. Collins, D. J.; Khoo, B. L.; Ma, Z.; Winkler, A.; Weser, R.; Schmidt, H.; Han, J.; Ai, Y., Selective particle and cell capture in a continuous flow using micro-vortex acoustic streaming. *Lab on a Chip* **2017,** *17* (10), 1769-1777.
56. Ma, Z.; Zhou, Y.; Collins, D. J.; Ai, Y., Fluorescence activated cell sorting via a focused traveling surface acoustic beam. *Lab on a Chip* **2017,** *17* (18), 3176-3185.
57. Shilton, R. J.; Travagliati, M.; Beltram, F.; Cecchini, M., Nanoliter- droplet acoustic streaming via ultra high frequency surface acoustic waves. *Advanced Materials* **2014,** *26* (29), 4941-4946.
58. Ding, X.; Li, P.; Lin, S.-C. S.; Stratton, Z. S.; Nama, N.; Guo, F.; Slotcavage, D.; Mao, X.; Shi, J.; Costanzo, F.; Huang, T. J., Surface acoustic wave microfluidics. *Lab on a Chip* **2013,** *13* (18), 3626-3649.
59. Collins, D. J.; Devendran, C.; Ma, Z.; Ng, J. W.; Neild, A.; Ai, Y., Acoustic tweezers via sub–time-of-flight regime surface acoustic waves. *Science Advances* **2016,** *2* (7), e1600089.
60. Devendran, C.; Gunasekara, N. R.; Collins, D. J.; Neild, A., Batch process particle separation using surface acoustic waves (SAW): integration of travelling and standing SAW. *RSC Advances* **2016,** *6* (7), 5856-5864.

61. Augustsson, P.; Karlsen, J. T.; Su, H.-W.; Bruus, H.; Voldman, J., Iso-acoustic focusing of cells for size-insensitive acousto-mechanical phenotyping. *Nature Communications* **2016,** *7*, 11556.
62. O'Rorke, R.; Collins, D.; Ai, Y., A rapid and meshless analytical model of acoustofluidic pressure fields for waveguide design. *Biomicrofluidics* **2018,** *12* (2), 024104.
63. Collins, D. J.; O'Rorke, R.; Devendran, C.; Ma, Z.; Han, J.; Neild, A.; Ai, Y., Self-Aligned Acoustofluidic Particle Focusing and Patterning in Microfluidic Channels from Channel-Based Acoustic Waveguides. *Physical Review Letters* **2018,** *120* (7), 074502.
64. Devendran, C.; Collins, D. J.; Ai, Y.; Neild, A., Huygens-Fresnel Acoustic Interference and the Development of Robust Time-Averaged Patterns from Traveling Surface Acoustic Waves. *Physical Review Letters* **2017,** *118* (15), 154501.
65. Collins, D. J.; Ma, Z.; Ai, Y., Highly Localized Acoustic Streaming and Size-Selective Submicrometer Particle Concentration Using High Frequency Microscale Focused Acoustic Fields. *Analytical Chemistry* **2016,** *88* (10), 5513-5522.
66. Muller, P. B.; Barnkob, R.; Jensen, M. J. H.; Bruus, H., A numerical study of microparticle acoustophoresis driven by acoustic radiation forces and streaming-induced drag forces. *Lab on a Chip* **2012,** *12* (22), 4617-4627.
67. Linic, S.; Aslam, U.; Boerigter, C.; Morabito, M., Photochemical transformations on plasmonic metal nanoparticles. *Nature Materials* **2015,** *14*, 567.
68. Arbabi, A.; Horie, Y.; Ball, A. J.; Bagheri, M.; Faraon, A., Subwavelength-thick lenses with high numerical apertures and large efficiency based on high-contrast transmitarrays. *Nature Communications* **2015,** *6*, 7069.
69. Kim, J.-W.; Jung, S.-B., Electrical Characterization of Screen-Printed Conductive Circuit with Silver Nanopaste. *Japanese Journal of Applied Physics* **2009,** *48* (6), 06FD14.
70. Lin, K.-H.; Lai, C.-M.; Pan, C.-C.; Chyi, J.-I.; Shi, J.-W.; Sun, S.-Z.; Chang, C.-F.; Sun, C.-K., Spatial manipulation of nanoacoustic waves with nanoscale spot sizes. *Nature Nanotechnology* **2007,** *2*, 704.
71. Ohlinger, A.; Deak, A.; Lutich, A. A.; Feldmann, J., Optically Trapped Gold Nanoparticle Enables Listening at the Microscale. *Physical Review Letters* **2012,** *108* (1), 018101.
72. Collins, D. J.; O'Rorke, R.; Neild, A.; Han, J.; Ai, Y., Acoustic fields and microfluidic patterning around embedded micro-structures subject to surface acoustic waves. *Soft Matter* **2019,** *15* (43), 8691-8705.
73. Wong, H. C.; Grenci, G.; Wu, J.; Viasnoff, V.; Low, H. Y., Roll-to-Roll Fabrication of Residual-Layer-Free Micro/Nanoscale Membranes with Precise Pore Architectures and Tunable Surface Textures. *Industrial & Engineering Chemistry Research* **2018,** *57* (41), 13759-13768.
74. Aran, K.; Sasso, L. A.; Kamdar, N.; Zahn, J. D., Irreversible, direct bonding of nanoporous polymer membranes to PDMS or glass microdevices. *Lab on a Chip* **2010,** *10* (5), 548-552.
75. Devendran, C.; Albrecht, T.; Brenker, J.; Alan, T.; Neild, A., The importance of travelling wave components in standing surface acoustic wave (SSAW) systems. *Lab on a Chip* **2016,** *16* (19), 3756-3766.
76. Bruus, H., Acoustofluidics 7: The acoustic radiation force on small particles. *Lab on a Chip* **2012,** *12* (6), 1014-1021.
77. Haslam, M. D.; Raeymaekers, B., Aligning carbon nanotubes using bulk acoustic waves to reinforce polymer composites. *Composites Part B: Engineering* **2014,** *60*, 91-97.
78. Collins, D. J.; Morahan, B.; Garcia-Bustos, J.; Doerig, C.; Plebanski, M.; Neild, A., Two-dimensional single-cell patterning with one cell per well driven by surface acoustic waves. *Nature Communications* **2015,** *6* (1), 8686.
79. Simon, G.; Andrade, M. A. B.; Reboud, J.; Marques-Hueso, J.; Desmulliez, M. P. Y.; Cooper, J. M.; Riehle, M. O.; Bernassau, A. L., Particle separation by phase modulated surface acoustic waves. *Biomicrofluidics* **2017,** *11* (5), 054115.
80. Glynne-Jones, P.; Boltryk, R. J.; Harris, N. R.; Cranny, A. W.; Hill, M., Mode-switching: A new technique for electronically varying the agglomeration position in an acoustic particle manipulator. *Ultrasonics* **2010,** *50* (1), 68-75.

81. Riaud, A.; Thomas, J.-L.; Charron, E.; Bussonnière, A.; Bou Matar, O.; Baudoin, M., Anisotropic Swirling Surface Acoustic Waves from Inverse Filtering for On-Chip Generation of Acoustic Vortices. *Physical Review Applied* **2015,** *4* (3), 034004.
82. Silva, G. T.; Lopes, J. H.; Leão-Neto, J. P.; Nichols, M. K.; Drinkwater, B. W., Particle Patterning by Ultrasonic Standing Waves in a Rectangular Cavity. *Physical Review Applied* **2019,** *11* (5), 054044.
83. Ding, X.; Lin, S.-C. S.; Kiraly, B.; Yue, H.; Li, S.; Chiang, I.-K.; Shi, J.; Benkovic, S. J.; Huang, T. J., On-chip manipulation of single microparticles, cells, and organisms using surface acoustic waves. *Proceedings of the National Academy of Sciences* **2012,** *109* (28), 11105-11109.
84. Brugger, M. S.; Grundeen, S.; Doyle, A.; Theogarajan, L.; Wixforth, A.; Westerhausen, C., Orchestrating cells on a chip: Employing surface acoustic waves towards the formation of neural networks. *Physical Review E* **2018,** *98* (1), 012411.
85. Chuo, S. T.-Y.; Chien, J. C.-Y.; Lai, C. P.-K., Imaging extracellular vesicles: current and emerging methods. *Journal of Biomedical Science* **2018,** *25* (1), 91.
86. Zijlstra, A.; Di Vizio, D., Size matters in nanoscale communication. *Nature Cell Biology* **2018,** *20* (3), 228-230.
87. Luo, M.; Epps, T. H., Directed Block Copolymer Thin Film Self-Assembly: Emerging Trends in Nanopattern Fabrication. *Macromolecules* **2013,** *46* (19), 7567-7579.
88. Cheng, W.; Park, N.; Walter, M. T.; Hartman, M. R.; Luo, D., Nanopatterning self-assembled nanoparticle superlattices by moulding microdroplets. *Nature Nanotechnology* **2008,** *3* (11), 682-690.
89. Cho, H.; Kim, J.; Park, H.; Won Bang, J.; Seop Hyun, M.; Bae, Y.; Ha, L.; Yoon Kim, D.; Min Kang, S.; Jung Park, T.; Seo, S.; Choi, M.; Suh, K.-Y., Replication of flexible polymer membranes with geometry-controllable nano-apertures via a hierarchical mould-based dewetting. *Nature Communications* **2014,** *5*, 3137.
90. Norland Optical Adhesive 73-SAFETY DATA SHEET. https://www.norlandprod.com/msds/noa%2073msd.html (accessed May 13, 2019).

TOC for smll.202000462

Interaction between a MHz travelling surface acoustic wave (SAW) and an elastic nanocavity layer at the interface of a microfluidic channel generates acoustically-driven oscillations in the nanocavities. The resultant nanoscale acoustic pressure gradients along the height of these nanocavities permit massively multiplexed sub-micron particle trapping within the nanocavities at the single-particle level.